



Simulation of curing process of carbon/epoxy composite during autoclave degassing molding by considering phase changes of epoxy resin



Seong-Hwan Yoo^{a, b}, Min-Gu Han^a, Jin-Ho Hong^a, Seung-Hwan Chang^{a, *}

^a School of Mechanical Engineering, Chung-Ang University (CAU), 221, Huksuk-Dong, Dongjak-Gu, Seoul 156-756, Republic of Korea

^b Korea Photonics Technology Institute Lighting Solution R&BD Center, Gwangju, Republic of Korea

ARTICLE INFO

Article history:

Received 1 December 2013

Received in revised form

7 March 2015

Accepted 11 March 2015

Available online 19 March 2015

Keywords:

A. Laminates

A. Polymer-matrix composites (PMCs)

B. Thermal properties

C. Finite element analysis (FEA)

ABSTRACT

Strain monitoring of a carbon/epoxy composite cross-ply laminate ($[0_5/90_5]_s$) during thermoforming was conducted by using fiber Bragg grating (FBG) sensors. The entire process was simulated by employing finite element analysis (FEA) by taking into consideration the phase changes of the epoxy resin. For the precise simulation of the curing process, a dielectrometry sensor was used to detect the epoxy-resin dissipation factor, which in turn was used to identify the curing point. To investigate the phase changes and consolidation of the composite laminate by employing FEA, modulus changes with temperature were measured by dynamic mechanical analysis (DMA), and the permeability was estimated by measuring the fiber volume fraction according to the curing temperature. As the epoxy resin changed from a liquid to solid phase, the strain generated along the carbon fibers dynamically changed, and the analysis results generally predicted the strain variation quite well. To apply this simulation technique to practical structures, a composite-aluminum hybrid wheel was analyzed and experimentally verified.

© 2015 Elsevier Ltd. All rights reserved.

1. Introduction

The excellent mechanical properties of fibrous composites have enabled them to be applied to the design of various structures, in which their performance has been closely investigated [1–3]. However, a variation in some factors, particularly, residual stress—a crucial factor—during the forming process may ultimately affect the performance of the final product. In order to investigate the effect of material behavior during a forming process on the performance of the final product, significant research on thermoforming processes has been conducted, e.g., on a smart cure cycle for controlling temperature overshoot [4], simulation techniques for composite laminates, incorporation of consolidation and thickness variation [5,6], and forming techniques that take the resin viscosity into account [7–9].

In addition, intensive research into different forming processes has also been carried out. An optimal cure cycle to minimize residual stress and strain has been previously proposed [10,11], with strain variation during thermoforming being observed and closely

investigated using fiber Bragg grating (FBG) optical sensors. This cycle takes into account the effect of thermal property differences between the composite laminate and the mold [12], the microstructures of fabric composites [13], boundary conditions [14], and differences in the coefficient of thermal expansion between different materials [15]. Health monitoring of composite structures [16,17] and cure monitoring of composite-metal hybrid structures [18,19] using various sensors have also been conducted to detect any material failures during service or forming conditions. Recently, the field of application of FBG sensors has been broadened to include real-time health monitoring of structures such as airplanes and ships [20–23]. The performance validation of FBG sensors, including their endurance limit, was also verified by comparing them with conventional sensors by performing various mechanical tests [24–29].

This paper presents the simulation of the curing of a carbon/epoxy laminate by taking into consideration the phase changes of the epoxy resin and the corresponding material property changes in the laminate. The strain and temperature change in the composite laminate was monitored during the curing process using FBG sensors, and the residual thermal strain also was measured. The simple technique for simulating the entire curing process with simple mechanical properties was developed using finite

* Corresponding author. Tel.: +82 2 820 5354; fax: +82 2 814 9476.

E-mail address: phigs4@cau.ac.kr (S.-H. Chang).

element analysis (FEA) with a user's subroutine, which predicted well the overall change in the generated strains in the composite laminate during the curing process. This technique may provide design guidance for composite structures, allowing durability to be enhanced by reducing the residual stress and strain of structures.

2. Experiments for determining parameters for the simulation

2.1. Materials and sensors

A carbon/epoxy prepreg (USN125, SK Chemical, Korea) was used to fabricate a laminate specimen. Vacuum bag degassing molding was then used to perform cure monitoring of the composite laminate, and all the materials used in the experiment are listed in Table 1. The material properties were obtained from a previous research [4–7].

Two types of sensors were used: FBG fiber optic sensors with an interrogator (Micron optics instrument, USA) were used for monitoring the strain and temperature of composite laminates during curing, and a dielectrometry sensor (see Fig. 1a; [11]) was used for detecting the degree of cure of the laminate. In order to accurately measure the strain variation with temperature in the composite laminate during curing, the sensor's coefficient of thermal expansion was compensated for in calculating equations:

$$\Delta\lambda_B = \lambda_0 \left[(\alpha_f + \xi) \Delta T + (1 - p_e) \Delta \varepsilon \right] = K_\varepsilon \Delta \varepsilon + K_T \Delta T \quad (1)$$

$$\Delta \varepsilon = \frac{\Delta\lambda_B - K_T \Delta T}{K_\varepsilon} \quad (2)$$

where $\Delta\lambda_B$, λ_0 , α_f , p_e , $\Delta \varepsilon$, ΔT , ξ , K_ε , and K_T are the wavelength shift, Bragg grating's peak reflection wavelength, FBG coefficient of thermal expansion (CTE), photo elastic constant of the optical fiber, strain change, temperature change of the FBG, Bragg grating's thermo-optical coefficient, sensitivity coefficient of strain, and sensitivity coefficient of temperature, respectively. The

dielectrometry sensor detects the mobility of dipoles and ions of liquid polymers during the curing process. This sensor submerged in the liquid polymer was represented as an equivalent circuit as shown in Fig. 1a. Based on the phase of the polymer, the dissipation factor (DF) can be calculated by Eq. (3):

$$DF = \frac{|I_R V_m|}{|I_C V_m|} = \frac{|I_R|}{|I_C|} = \frac{|Z_C|}{|Z_R|} = \frac{1}{\omega R_m C_m} \quad (3)$$

where I , Z , V_m , R_m , and C_m are the electric current, equivalent impedance, supplied voltage (which varies with the supplied frequency), equivalent resistance, and equivalent capacitance, respectively. The subscripts R and C represent the resistance and capacitance, respectively.

2.2. Measurement of the fiber volume fraction

To estimate the amount of resin extracted during vacuum bag degassing molding, the fiber volume fraction according to temperature was measured. Darcy's law [7] predicts the resin flow during the curing of composites based on the permeability (k_i) of the material, and it is closely related to the material void ratio [30] (e ; Eq. (4)):

$$e = \frac{\text{Vol} - \text{Vol}_f}{\text{Vol}_f} = \frac{\text{Vol}}{\text{Vol}_f} - 1 = \frac{1}{\text{Vol}_f} - 1 \quad (4)$$

where Vol and Vol_f represent respectively the total volume and fiber volume of the composite laminate. At every target temperature, the mass of the composite laminate was measured, with the fiber mass also being measured after burning the matrix of the laminate. Based on the Kozeny–Carman theory [7], the permeability (k_i) can be expressed in terms of the void ratio (e):

$$k_i = \frac{r_f^2}{4c_i} \frac{e^3}{(1+e)} \quad (5)$$

where r_f and c_i are the fiber radius and Kozeny–Carman constant, respectively. The permeability of the composite laminate

Table 1
Material properties and measured values of various materials.

	Materials	Thermal conductivity (W/mK)		Specific heat capacity (J/kg K)		Density (kg/m ³)		
Mechanical properties	Epoxy	0.2		1740		1210		
	Fiber	85.0		700		1750		
	Steel	60.0		450		8000		
	Vacuum bag	0.24		1670		1140		
	Breather	0.007		1350		260		
	Teflon film	0.4		1050		2200		
	Materials	Density (kg/m ³)	Young's Modulus (GPa)		Poisson's ratio		Elongation (%)	
Mechanical properties	USN125	1480	E_1	131.0	ν_{12}	0.0226	1.8	
			E_2	10.5	ν_{23}	0.0226		
			E_3	10.5	ν_{31}	0.4700		
	Aluminum	2700	68.9		0.33		17.0	
	Materials	125 °C		105 °C	85 °C	65 °C	45 °C	25 °C
CTE for temperature (10 ⁻⁶ /°C)	USN125	L	-2.21	-1.85	-1.66	-1.49	-1.31	-1.09
		T	62.82	48.42	37.44	29.79	25.20	23.80
	Aluminum	23.76	23.49	23.29	23.09	22.91	22.86	
	Steel	12.82	12.40	12.24	12.02	11.72	11.56	
	Temperature (°C)		Fiber volume fraction			Permeability		
V_f and permeability for temperature	25		0.55			0.8181		
	55		0.56			0.7857		
	80		0.58			0.7241		
	100		0.60			0.6666		
	125		0.61			0.6339		

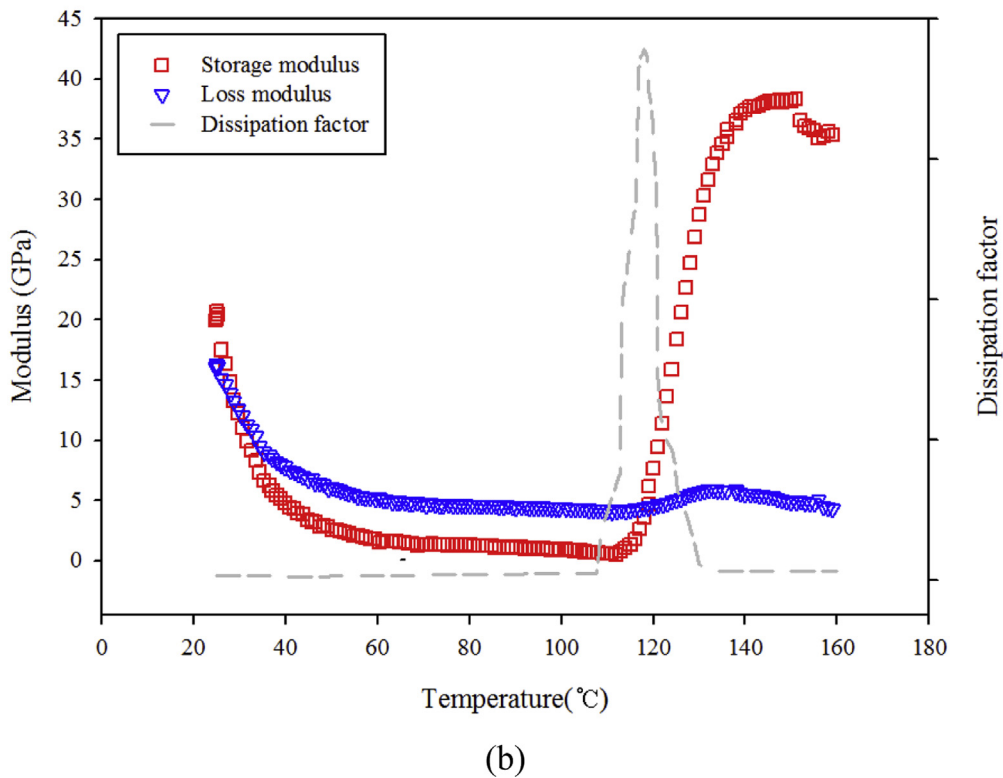
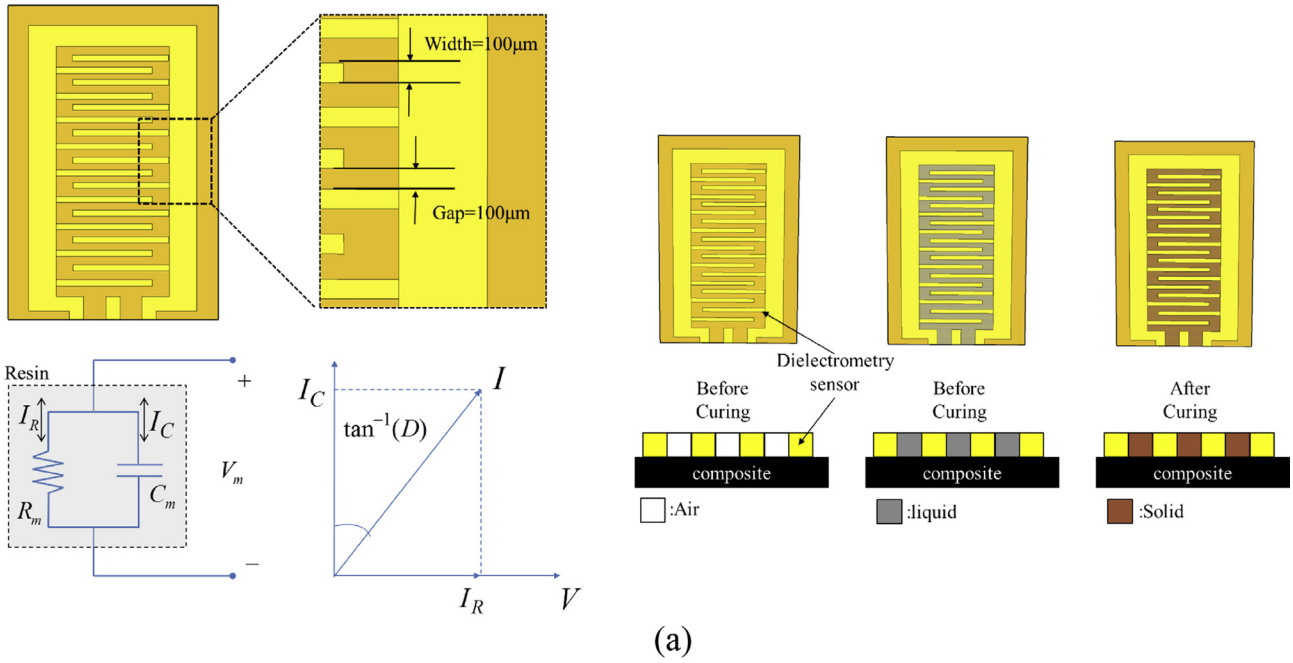


Fig. 1. Property variation of carbon/epoxy prepreg: (a) dielectrometry sensor and corresponding equivalent circuit and (b) variation of moduli and dissipation factor with temperature.

corresponding to the forming temperature was calculated using Eq. (5), and the values are listed in Table 1. This permeability was used to simulate the thermoforming process of the composite laminates, based on previously identified resin flow behavior [5,7,9]. The fiber volume fraction was saturated at a value of 0.61 when the test temperature reached 125 °C, generating a saturated permeability of 0.6339. Beyond this point, the epoxy resin was regarded as having entered the gelation phase.

2.3. Dynamic mechanical analysis (DMA)

Storage and loss moduli of the composite laminates at different temperatures were measured by a Dynamic Mechanical Analysis (DMA) machine (Triton Technology, UK). A short beam specimen of stacked carbon/epoxy prepregs was mounted on the machine, and the test temperature was raised to 160 °C at a rate of 1 °C/min, with a driving frequency of 1 Hz. The measured moduli are plotted in

Fig. 1b, and this data was subsequently used to simulate the forming process.

2.4. Strain measurement of a carbon/epoxy laminate during thermoforming

Real time in-situ strain variation in a composite laminate during vacuum bag degassing molding was investigated experimentally using FBG fiber optic sensors. The stacking sequence of the laminate was $[0_5/90_5]_s$, and sensors were inserted between the third and the fourth plies along the 0° fibers, and 10th and 11th plies along the 90° fibers, as illustrated in Fig. 2a. A dielectrometry sensor was also inserted at the edge of the laminate. A pair of steel plates was then applied to the laminate, and various accessories such as a Teflon film were applied to both surfaces as shown in Fig. 2a. In order to ensure easy demolding of the composite laminate, a releasing agent was sprayed onto the surfaces of the steel mold. Wavelength shifts, which can be used to calculate strain using Eqs. (1) and (2), were measured for different forming time by an interrogator. In addition, the equivalent resistance and capacitance of the epoxy-impregnated dielectrometry sensor (see Fig. 1a) were measured by an LCR meter, and these values were substituted in Eq. (3) to calculate DF. The temperature was also measured by the FBG sensor in the composite laminate. The recommended cure cycle is shown in Fig. 2b. These measured strains were used for the verification of the simulation technique and its accuracy.

3. Simulation of the curing process using finite element analysis

To estimate the strain variation during the thermoforming of a carbon/epoxy laminate, FEA was conducted using the experimentally acquired data introduced in Section 2, such as the permeability (k_i) and modulus at various forming temperatures. These results were later being compared against the cure monitoring test results for verifying the appropriateness of the simulation technique. The finite element model of the laminate is shown in Fig. 3a. A commercial finite element code—ABAQUS 6.11 with C3D8HT element—was used, with the number of elements set to 14,400. The analysis process itself was divided into three phases (Phases I, II, III) based on the different phases of the epoxy resin: Phase I (heating: 25°C to 125°C) is for the liquid phase, Phase II (holding: 125°C) is for the gelation of the epoxy resin, and Phase III (cooling: 125°C to room temperature) is the solidification phase of the epoxy resin, including vitrification. In Phase I, the deformation behavior of the composite laminate was investigated by taking into account the variation in permeability and the modulus of the laminate. To determine the change in permeability by employing FEA, the VOIDRI code provided by ABAQUS was used. Iterative calculation of the generated strain (see Fig. 3b) was carried out by varying the permeability and modulus of the composite laminates. The material properties and permeability corresponding to the forming temperatures were updated, and once the permeability reached a value of 0.6339, the gelation phase of the epoxy resin was considered to have commenced and the iteration process was terminated. As gelation proceeded in Phase II, the Poisson's ratio of the epoxy resins increased [31] to a point (0.48) at which they could be regarded as a rubber-like hyperelastic material. The permeability and Young's modulus at a temperature of 125°C were used for calculating strains in the laminate. In those phases (Phase I and Phase II) Mooney–Rivlin model was used to simulate the strains to cope with non-linear behavior of epoxy resin as a hyperelastic material and storage moduli according to temperature measured by DMA were used. The VOIDRI code which is able to express resin

flow based on Darcy's law was used to determine the material state when the composite laminate was in liquid state. According to the permeability variation of the epoxy resin at a certain temperature appropriate storage modulus was assigned in each FE element by VOIDRI code and the iterative calculation was carried out as shown in Fig. 3b.

In Phase III, changes in the coefficient of thermal expansion and Young's modulus of the cured composite laminate were used in the FEA for precise estimation of strain as done in a related study [32]. Simple Hooke's law was used to calculate material strains because in this phase the laminate was solid state.

A tie condition between the laminate and steel mold was imposed for Phase I and II analyses resulting in the same strain at the interface, and a contact condition with a friction coefficient of 0.2 was applied at the interface between the laminate and steel mold, taking into account the partial demolding that occurred under abrupt temperature changes. And one node at the edge of the FE model was fixed in all directions for the convergence. As a loading condition hydrostatic compression of 0.1 MPa (vacuum) was applied to the FE model.

4. Verification of the simulation technique

4.1. Experiments for strain monitoring during curing process

Fig. 4 shows the results of cure monitoring experiments and analyses, in which the strain was measured in 0° and 90° plies along the fibers. To identify the epoxy-resin phase changes corresponding to the curing time, DF was plotted and analyzed along with the strain variation around the onset of phase change of the epoxy resin. The DF and the measured strain were subsequently used to classify the resin phases, as shown in Fig. 4a–b. The border between Phase I (liquid regime) and Phase II (gelation regime) is identified by a peak in the DF value, which is indicative of large-scale cross-linking in the epoxy resin.

4.1.1. Phase I

In Phase I, the liquefied epoxy resin shrinks under vacuum (hydrostatic compression of 0.1 MPa), generating a negative strain of $-230\mu\epsilon$ and $-223\mu\epsilon$, in 0° and 90° plies, respectively, which follows a trend similar to that observed in previous studies [11,12]. The gradual reduction in the viscosity of the epoxy resin with increasing temperature induces a corresponding negative strain, and this trend abruptly reverses with the instantaneous curing of the epoxy resin; i.e., around the peak DF value, the strain exhibits a minimum value, as shown in Fig. 4a–b.

4.1.2. Phase II

In Phase II, the gelated epoxy resin behaves like rubber stuck to the mold surface, causing compressive strain in the thickness direction and in-plane tensile strain under vacuum conditions. At a constant temperature (125°C), the strain linearly increased with time up to the vitrification of the epoxy resin, as shown in Fig. 4a–b. Consolidation of the laminate continued to occur during this period, which reduced the thickness and resulted in extension along the in-plane direction due to the high Poisson's ratio (0.48). In experiments, maximum tensile strain values of $300\mu\epsilon$ and $330\mu\epsilon$ were measured in the 0° and 90° plies, respectively.

4.1.3. Phase III

In Phase III, vitrification was observed around 15 min prior to the commencement of the cooling process. However, this short regime of vitrification was sufficient for the epoxy resin to completely solidify and become hardened. During this phase, the rate of strain

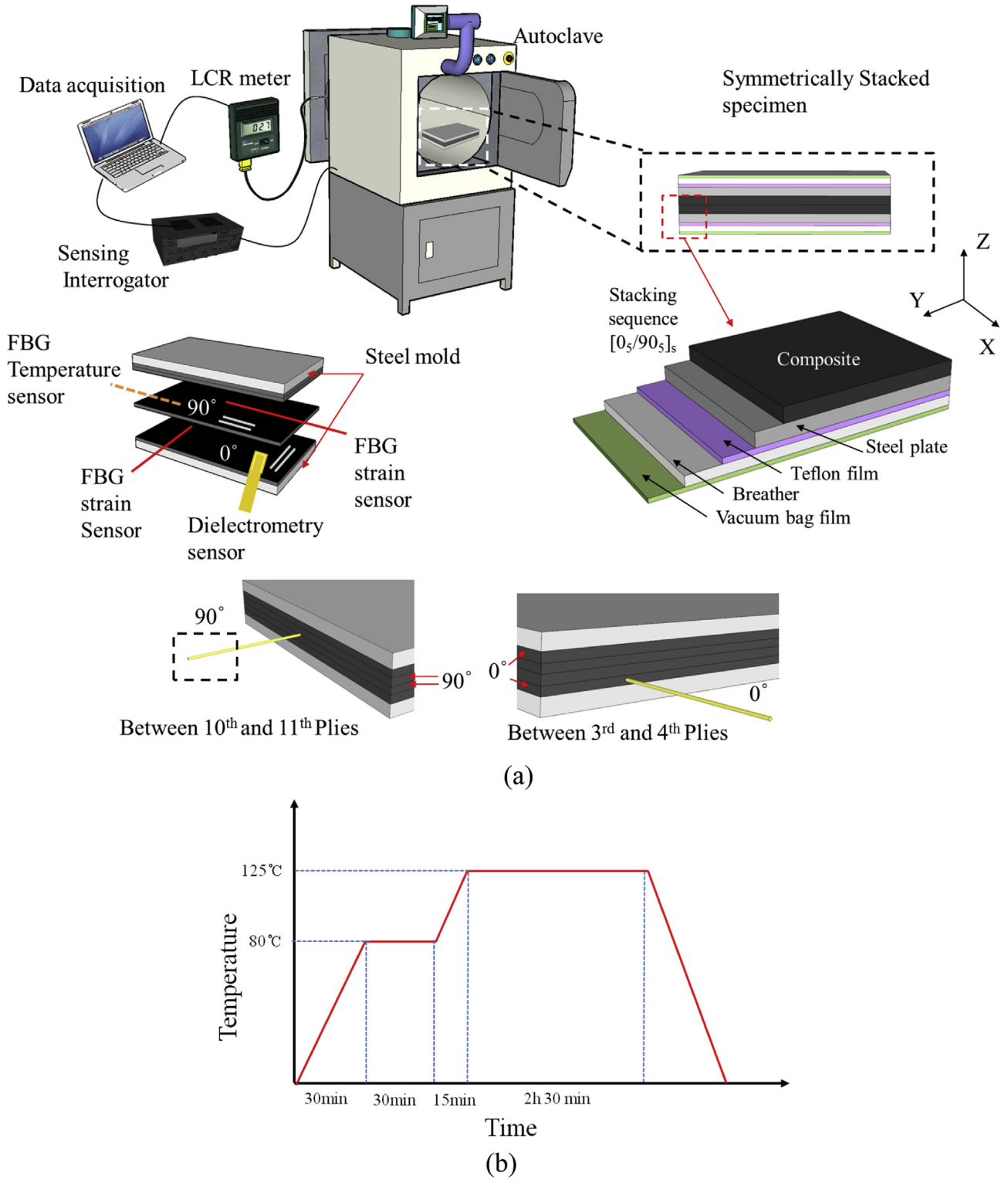


Fig. 2. Details of cure monitoring of a composite laminate and sensor configuration: (a) preparation for thermoforming of a laminate and (b) recommended cure cycle.

increase first reduced and then abruptly decreased with the onset of cooling. This is presumably caused by stick-slip motion (partial delamination) at the interface between the composite laminate and the steel mold, due to the significant difference in thermal expansion coefficients of both materials ($-0.9 \mu\text{m}/\text{m}^\circ\text{C}$ for 0° ply and $13 \mu\text{m}/\text{m}^\circ\text{C}$ for a steel mold) under abrupt cooling conditions [12,14,15] (see Fig. 4b).

In Phase III, the thermal residual strain was defined by the difference between the peak strain in Phase II and the strain when the cooling process was terminated. As shown in Fig. 4, the laminate strain decreased as the cooling process proceeded, eventually reaching $-157\mu\epsilon$ and $-72\mu\epsilon$ in 0° and 90° plies, respectively. Consequently, the generated thermal residual strain was $-253\mu\epsilon$ and $-160\mu\epsilon$ in the 0° and 90° plies, respectively.

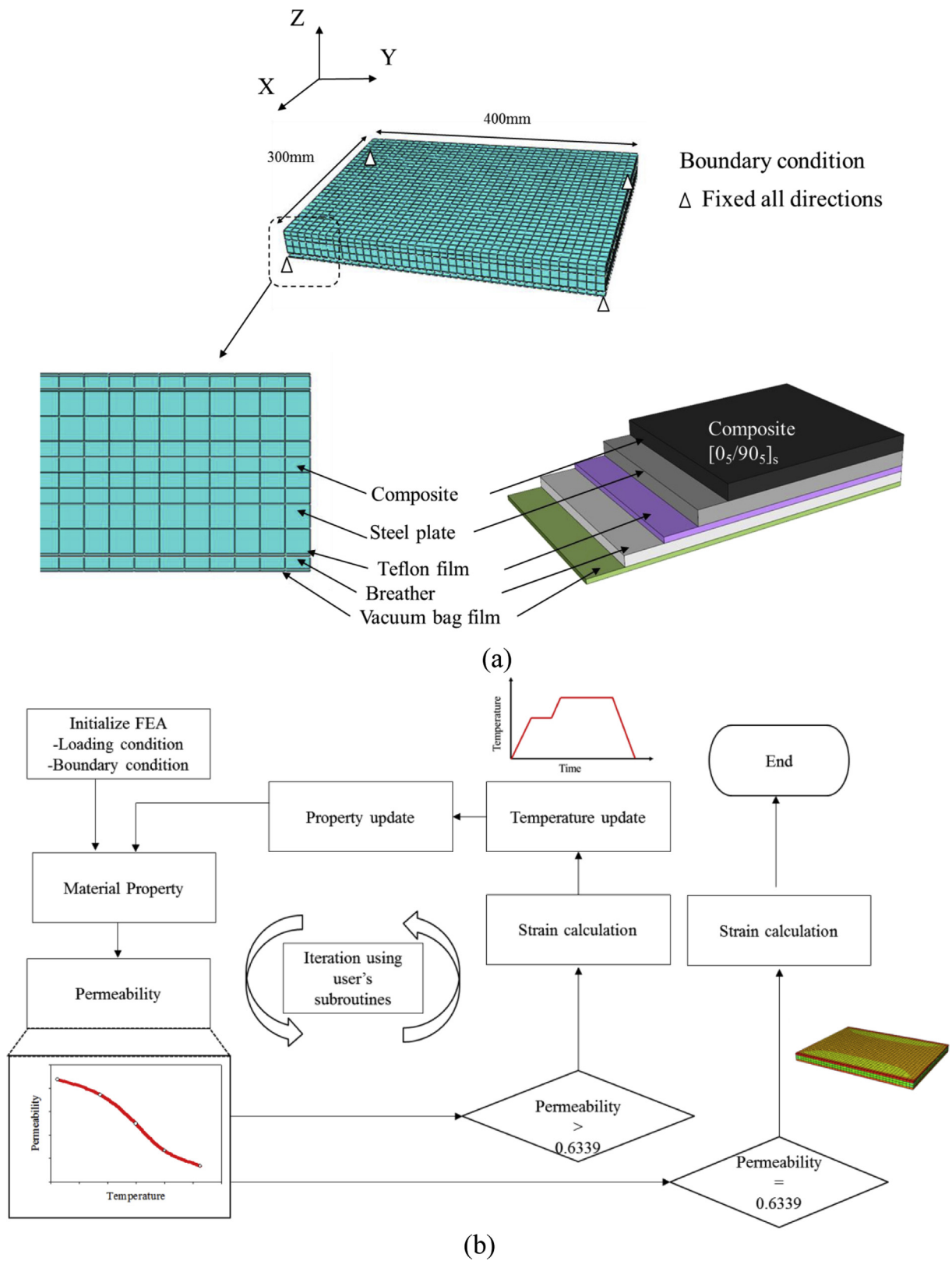


Fig. 3. Finite element analysis of the curing process of a composite laminate: (a) finite element model and (b) analysis procedure.

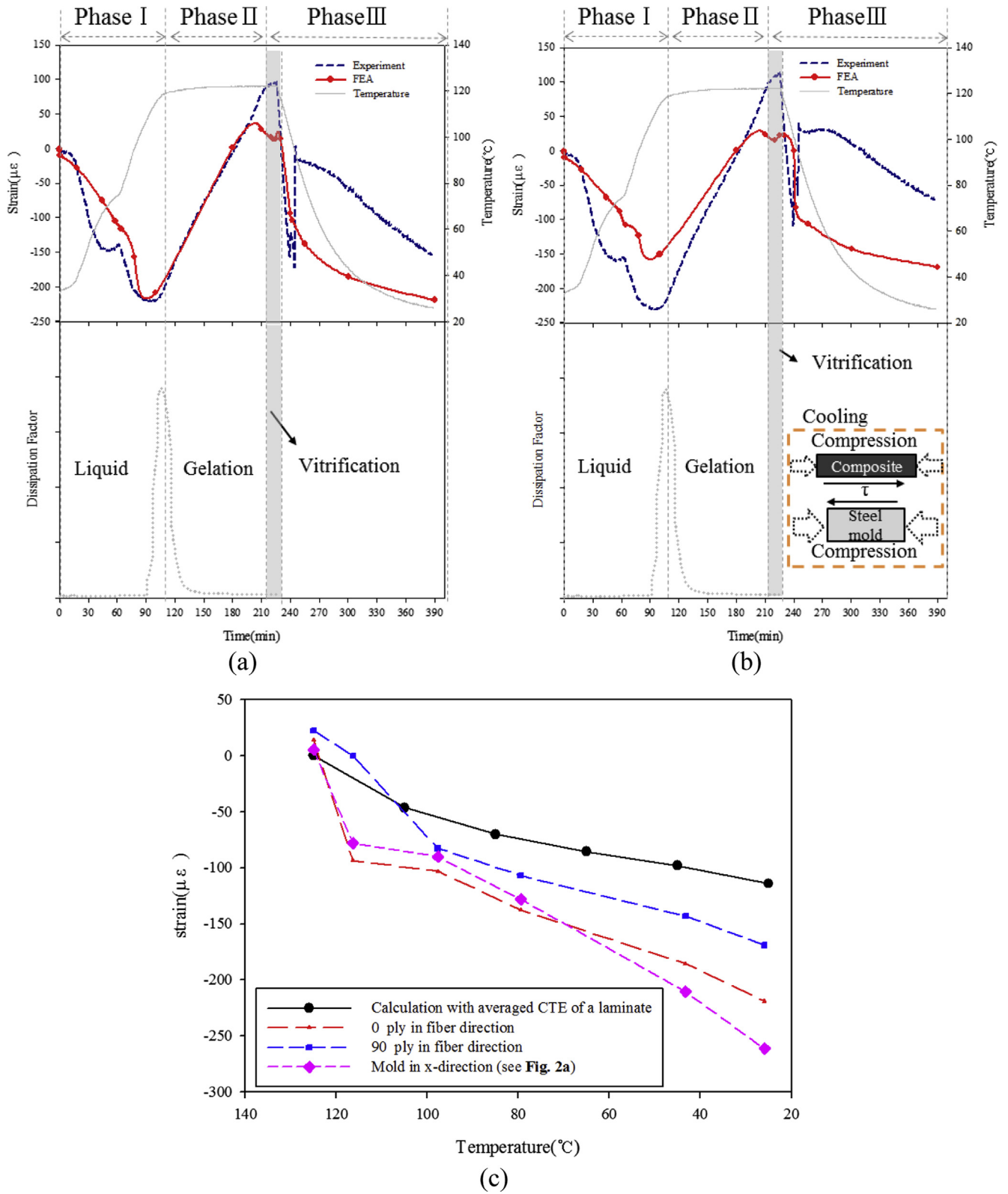


Fig. 4. Strain monitoring results: (a) 0° ply along the fiber direction, (b) 90° ply along the fiber direction, and (c) strain variation in materials during cooling (Phase III).

4.2. Simulation of strain variation during the curing process

4.2.1. Phase I

Finite element analysis predicted well the behavior of the laminate under compression, showing the minimum strains of $-210\mu\epsilon$ and $-154\mu\epsilon$ in the 0° and 90° plies, respectively. The relatively substantial difference between the experimentally determined and calculated strain values of the 90° ply that was located in the center of the laminate (see Fig. 2a), presumably comes from the large degree of deformation caused by resin flow during this period when the analysis could not accurately simulate the precise mass transfer (see Fig. 4b). Consequently, FEA with a linear element underestimates the deformation of epoxy in this phase.

4.2.2. Phase II

In analyses, a maximum tensile strain of $221\mu\epsilon$ and $172\mu\epsilon$ was measured in the 0° and 90° plies, respectively. The relatively large error (36% and 48%) between the experimentally measured and analyzed results comes from the simplified analysis that only considers the laminate's mechanical behavior corresponding to changes in permeability and does not consider factors such as the chemical behavior of the epoxy resin and the interaction between the mold and the laminate [12]. However, the overall trends of strain variation as per the simulation and measured results were similar.

4.2.3. Phase III

In Phase III, the terminal strains calculated by FEA were $-218\mu\epsilon$ and $-170\mu\epsilon$ in 0° and 90° plies, respectively. Consequently, the simulated thermal residual strain was $-229\mu\epsilon$ and $-188\mu\epsilon$ in the 0° and 90° plies, respectively, which were quite well estimated by the simulation.

4.3. Evaluation of the simulation in terms of the residual strain

The 90° plies had a relatively low residual strain owing to their location in the center part of the laminate, which was little affected by steel molds having a much higher CTE ($13\mu\text{m}/\text{m}^\circ\text{C}$); on the other hand, the CTE of the fiber direction of carbon/epoxy prepreg is $-0.9\mu\text{m}/\text{m}^\circ\text{C}$. On the other hand, the 0° plies were significantly affected by the mold, since they were in direct contact with it (see Fig. 4c). The composite laminate with a stacking sequence of $[0_5/90_5]_s$ has an averaged CTE of $2.52\mu\text{m}/\text{m}^\circ\text{C}$ in orthotropic directions; when this averaged CTE is used to calculate strains, it is expected to produce low magnitudes of strain in FEA, as shown in Fig. 4c. However, from a microscopic point of view, there was strain variation along the thickness direction based on the stacking angle of each ply (see Fig. 4c). Therefore, even though the FBG sensor embedded along the fibers tends not to deform the adjacent layers, a difference in CTE along a certain direction (including the steel mold) significantly affects the interaction of certain plies with the sensor, thus resulting in the thermal residual strain in each ply that is shown in Fig. 4.

From the results of this experimental work and the FEA, the type and level of generated strain during curing was identified and this information may be used to develop a means to reduce thermal residual stress or strain of composite structures by modifying their cure cycle. Through this study, the validity of the simulation technique based on FEA was verified, and its suitability for application to the design of any composite structure was established.

5. Engineering practice: simulation of thermoforming of a composite-aluminum hybrid wheel

5.1. Simulation

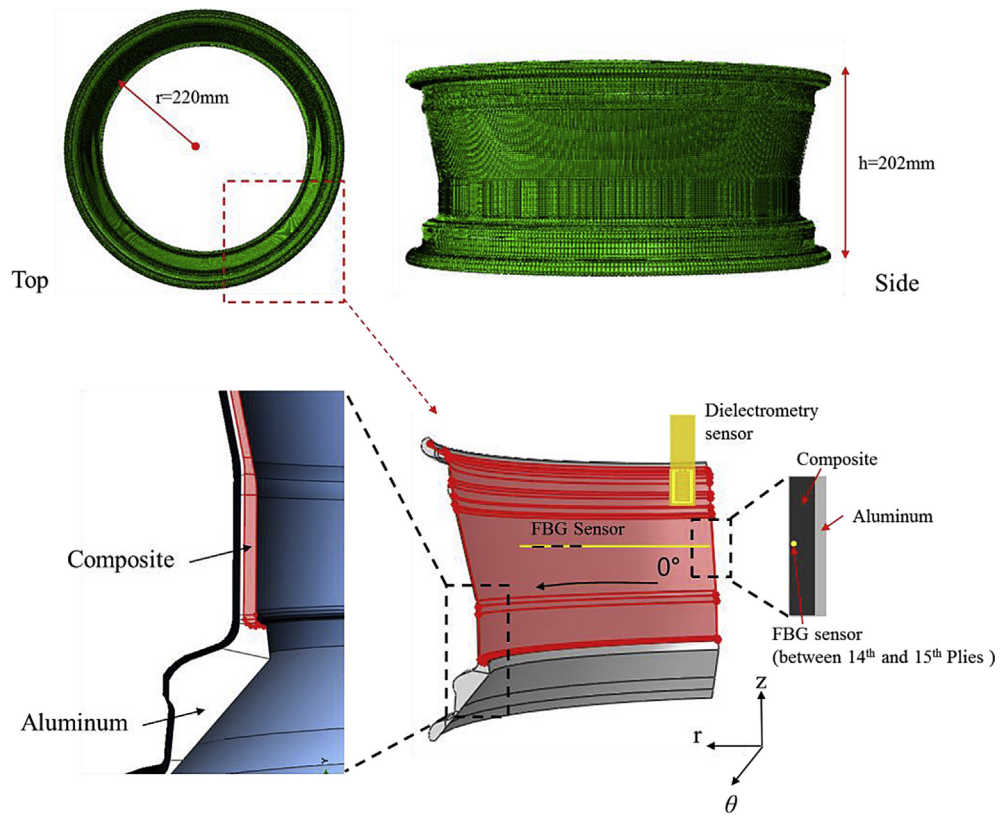
To apply the simulation technique to a real composite structure, a composite-aluminum hybrid wheel for a passenger car was selected and the strain variation during thermoforming was measured and evaluated. It is hoped that the results will provide a design guideline for reducing or optimally utilizing the residual stress and strain for realizing better performance in such structures [9,33]. The overall shape and dimensions of the structure are shown in Fig. 5, and the material properties are listed in Table 1. For the simulation of strain during the thermoforming of the hybrid wheel, only a quarter section of the wheel circumference was modeled with surface symmetry at the cutting surfaces. All simulation techniques and procedures were the same as those introduced in section 3 for the composite laminate.

5.2. Experiments

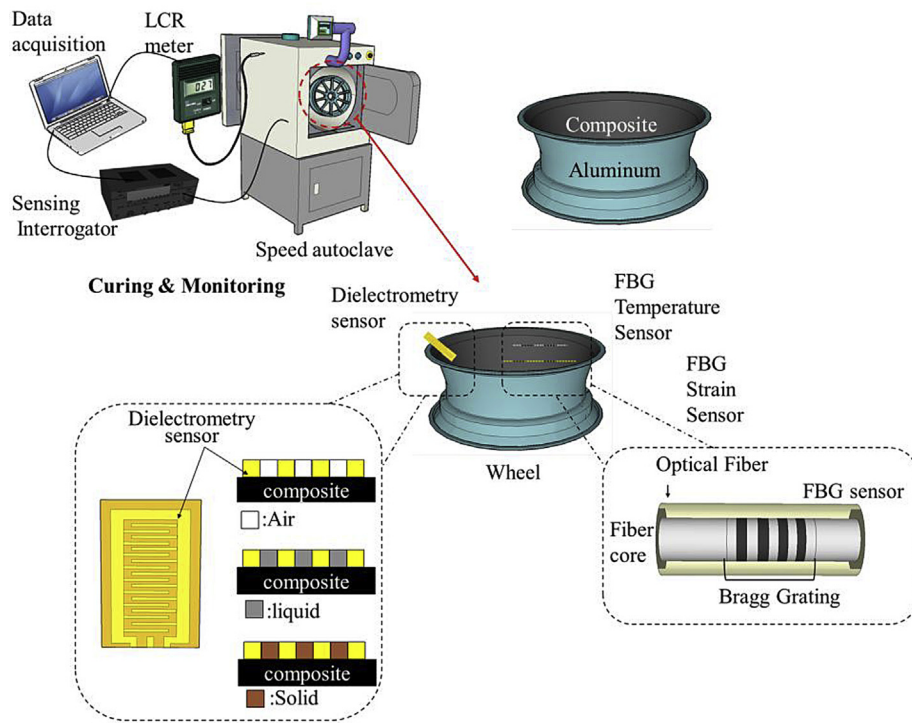
For the experimental evaluation, 16 plies of carbon/epoxy prepregs (USN125, SK Chemical, Korea) were stacked inside the aluminum part of a wheel along the hoop direction (0°) along the circumference, as shown in Fig. 5a. An FBG sensor was inserted along the direction of the fibers between the 14th and 15th plies from the aluminum surface, and a dielectrometry sensor was also inserted into the composite part to monitor the strain and DF (see Fig. 5a–b). The forming conditions were the same as those in the case of the composite laminate, with the composite and aluminum parts being bonded by co-cure bonding. The major differences between these two cases were the topology of the structure and the bonding characteristics; i.e., the hybrid wheel had a closed form with co-cure bonding between the composite and aluminum, while the composite laminate had an open structure with a very weak bonding with the steel mold because of the releasing agent used. These differences generated different behaviors in the composite part during the cooling phase (Phase III).

5.3. Evaluation and discussion

Fig. 6a shows the measured and analyzed strain during the thermoforming of the hybrid wheel, from which it can be seen that in Phases I and II, the trend of strain along fibers is the same as that in the case of composite laminate, as shown in Figs. 4 and 6. The analysis predicted well the generated strain by considering the variation in permeability with temperature. As consolidation of the stacked prepregs proceeds, the strain gradually increases due to the high Poisson's ratio of the gelled epoxy under vacuum conditions. In Phase III, the factors affecting the variation in the magnitude and type of strain generated were many, including contact conditions, anisotropic thermal properties of the composite, interactions with the aluminum part, and chemical reactions such as the cure shrinkage of epoxy resin [34]. The initial strain peak in the cooling phase presumably comes from the negative CTE ($-0.9\mu\text{m}/\text{m}^\circ\text{C}$) of the composite, which was abruptly exposed to room temperature by opening of the autoclave. Beyond this point, the strain gradually drops due to the shrinkage of the outer aluminum rim with a high CTE ($23.76\mu\text{m}/\text{m}^\circ\text{C}$), which generates radial pressure between the composite and rim parts (see Fig. 6b). The strain peak at the beginning of the cooling phase (Phase III) was not accurately predicted by the analysis because the analysis could not predict the local microscopic deformation of the composite but simply estimated the macroscopic behavior by considering the interaction between the



(a)



(b)

Fig. 5. Cure monitoring of a composite-aluminum hybrid wheel: (a) shape and dimensions and (b) details of cure monitoring.

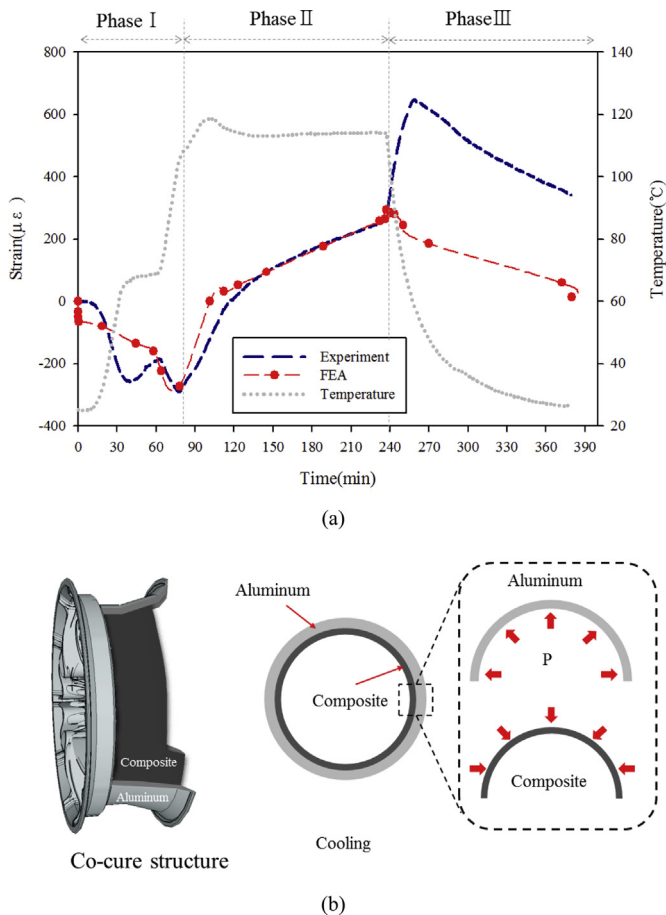


Fig. 6. Strain monitoring results: (a) measured and calculated strain along the fiber direction and (b) illustration of the generated pressure between two materials due to thermal residual stress.

aluminum and composite parts. On the other hand, in experiments, an FBG sensor was inserted into the outer layers of the composite, thereby allowing local deformation of adjacent layers of the composite laminate to be detected with minimal effect on the aluminum part. This is currently a limitation of the current FE model, which needs to be resolved for accurate analysis especially in the case of complex structures. However, from a qualitative point of view the results reveal that the composite part exhibited tensile strain under a compressive stress environment, which means that the entire structure expanded while the outer aluminum rim still provided pressure to the composite part. Such conditions enhance the fatigue strength of the structure, and therefore this simulation technique can be used to predict the level of residual strain. Furthermore, it also allows for optimal forming processes to be developed, thus leading to better structural design.

6. Conclusion

Strain variation in a carbon/epoxy composite laminate ($[0_5/90_5]_s$) during thermoforming was simulated by finite element analysis, and for verification, the generated strain was also monitored by employing fiber Bragg grating sensors. The generated strain varied dynamically as the phase of the epoxy resin changed from liquid to solid via a gel. The onset of the gelation point was detected by a dielectrometry sensor and indicated by the variation in strain. To simulate the strain variation accurately, the modulus

variation with temperature of carbon/epoxy prepregs was measured by a performing dynamic mechanical analysis, and the variation in fiber volume fraction with temperature was measured to calculate the permeability of the composite. Based on the variation in strain and the dissipation factor, the cure process was classified by the three phases: Phase I (liquid), Phase II (gelation), and Phase III (vitrification and solidification). Overall, the simulated strain agreed well with the measured values, but a relatively big difference was observed at the phase changing points (liquid to gel), especially with the 90° ply. This difference is presumed to have come from the large deformation of the ply caused by resin flow during this period, when the analysis could not simulate the exact mass transfer and substantial deformation. In addition, the substantial difference observed between Phase II and Phase III (gel to solid) was because of the simplified analysis that does not consider the chemical behavior of the epoxy resin or the interaction between the mold and the laminate. This is a drawback of the current FE model, which is yet to be addressed.

Applying the simulation technique to a composite-aluminum hybrid structure produced results similar to those for the composite laminate in Phases I and II; however, an abrupt increase in strain was observed from the beginning of cooling phase (Phase III), which is opposite to the trend observed in the laminate. This difference in behavior came about from the difference in the topology of the two structures: i.e., an open shape for the laminate, and closed shape for the wheel. Again, the abrupt strain change at the beginning of cooling was not effectively simulated for the same reasons as those in the case of the composite laminate. However, the simulation did successfully estimate the trend of strain variation and the level of residual strain, which affects the static and fatigue strengths of composite structures. This simulation technique may therefore provide a useful means to reduce residual stress by changing the forming process, and enhancing the structural integrity of composite structures.

References

- [1] Yoo SH, Chang SH, Sutcliffe MPF. Compressive characteristics of foam-filled composite egg-box sandwich panels as energy absorbing structures. *Compos Part A-Appl Sci* 2010;41(3):427–34.
- [2] Chung JG, Chang SH. Changes in tow geometry of plain-weave carbon/epoxy fabrics draped onto compliant hemisphere molds. *Polym Compos* 2006;27(2):111–8.
- [3] Yoo SH, Park SW, Chang SH. An experimental study on the effect of tow variations on compressive characteristics of plain weave carbon/epoxy composites under compressions. *Compos Struct* 2010;92(3):736–44.
- [4] Oh JH, Lee DG. Cure cycle for thick glass/epoxy composite laminates. *J Compos Mater* 2002;36(1):19–45.
- [5] Young WB. Consolidation and cure simulations for laminated composites. *Polym Compos* 1996;17(1):142–8.
- [6] Blest DC, Duffy BR, McKee S, Zulkiflfe AK. Curing simulation of thermoset composites. *Compos Part A-Appl Sci* 1999;30(11):1289–309.
- [7] Lee DG, Kim JS. Computer simulation of the consolidation of fiber reinforced resin matrix composites. *J Mater Process Manuf Sci* 1994;2(4):357–72.
- [8] Kiuna N, Lawrence CJ, Fontana QPV, Lee PD, Selerland T, Spelt PDM. A model for resin viscosity during cure in the resin transfer moulding process. *Compos Part A-Appl Sci* 2002;33(11):1497–503.
- [9] Laurenzi S, Grilli A, Pinna M, De Nicola F, Cattaneo G, Marchetti M. Process simulation for a large composite aeronautic beam by resin transfer molding. *Compos Part B-Eng* 2014;57:47–55.
- [10] Agius SL, Magniez KJC, Fox BL. Cure behaviour and void development within rapidly cured out-of-autoclave composites. *Compos Part B-Eng* 2013;47:230–7.
- [11] Kim HS, Yoo SH, Chang SH. In situ monitoring of the strain evolution and curing reaction of composite laminates to reduce the thermal residual stress using FBG sensor and dielectrometry. *Compos Part B-Eng* 2013;44(1):446–52.
- [12] Mülle M, Collombet F, Olivier P, Grunevald YH. Assessment of cure residual strains through the thickness of carbon-epoxy laminates using FBGs, Part I: Elementary specimen. *Compos Part A-Appl Sci* 2009;40(1):94–104.
- [13] Daggumati S, Voet E, Van Paepegem W, Degrieck J, Xu J, Lomov SV, et al. Local strain in a 5-harness satin weave composite under static tension: Part I - experimental analysis. *Compos Sci Technol* 2011;71(8):1171–9.

- [14] Sorensen L, Gmur T, Botsis J. Residual strain development in an AS4/PPS thermoplastic composite measured using fibre Bragg grating sensors. *Compos Part A-Appl Sci* 2006;37(2):270–81.
- [15] Twigg G, Poursartip A, Fernlund G. An experimental method for quantifying tool-part shear interaction during composites processing. *Compos Sci Technol* 2003;63(13):1985–2002.
- [16] Kang DH, Kim CU, Kim CG. The embedment of fiber Bragg grating sensors into filament wound pressure tanks considering multiplexing. *NDT E Int* 2006;39(2):109–16.
- [17] Archer E, Broderick J, McIlhagger AT. Internal strain measurement and cure monitoring of 3D angle interlock woven carbon fibre composites. *Compos Part B-Eng* 2014;56:424–30.
- [18] Kwon JW, Chin WS, Lee DG. In situ cure monitoring of adhesively bonded joints by dielectrometry. *J Adhes Sci Technol* 2003;17(16):2111–30.
- [19] Kim HS, Lee DG. Reduction of fabrication thermal residual stress of the hybrid co-cured structure using a dielectrometry. *Compos Sci Technol* 2007;67(1):29–44.
- [20] Palaniappan J, Ogin SL, Thorne AM, Reed GT, Crocombe AD, Capell TF, et al. Disbond growth detection in composite-composite single-lap joints using chirped FBG sensors. *Compos Sci Technol* 2008;68(12):2410–7.
- [21] Herszberg I, Li HCH, Dharmawan F, Mouritz AP, Nguyen M, Bayandor J. Damage assessment and monitoring of composite ship joints. *Compos Struct* 2005;67(2):205–16.
- [22] Silva-Munoz RA, Lopez-Anido RA. Structural health monitoring of marine composite structural joints using embedded fiber Bragg grating strain sensors. *Compos Struct* 2009;89(2):224–34.
- [23] Baker W, Mckenzie I, Jones R. Development of life extension strategies for Australian military aircraft, using structural health monitoring of composite repairs and joints. *Compos Struct* 2004;66(1–4):133–43.
- [24] Leng J, Asundi A. Structural health monitoring of smart composite materials by using EPFI and FBG sensors. *Sens Actuat A-Phys* 2003;103(3):330–40.
- [25] Pereira G, Frias C, Faria H, Frazao O, Marques AT. On the improvement of strain measurements with FBG sensors embedded in unidirectional composites. *Polym Test* 2013;32(1):99–105.
- [26] Lau KT, Yuan LB, Zhou LM, Wu JS, Woo CH. Strain monitoring in FRP laminates and concrete beams using FBG sensors. *Compos Struct* 2001;51(1):9–20.
- [27] De Baere I, Luyckx G, Voet E, Van Paepegem W, Degrieck J. On the feasibility of optical fibre sensors for strain monitoring in thermoplastic composites under fatigue loading conditions. *Opt Laser Eng* 2009;47(3–4):403–11.
- [28] Kerrouche A, Boyle WJO, Sun T, Grattan KTV, Schmidt JW, Taljsten B. Enhanced FBG sensor-based system performance assessment for monitoring strain along a prestressed CFRP rod in structural monitoring. *Sens Actuat A-Phys* 2009;151(2):127–32.
- [29] Dawood TA, Shenoi RA, Sahin M. A procedure to embed fibre Bragg grating strain sensors into GFRP sandwich structures. *Compos Part A-Appl Sci* 2007;38(1):217–26.
- [30] ASTM D2734-94. Standard test methods for void content of reinforced plastics. American Society for Testing and Materials International; 2009.
- [31] Plepys AR, Farris RJ. Evolution of residual-stresses in 3-dimensionally constrained epoxy-resins. *Polymer* 1990;31(10):1932–6.
- [32] Yoon KJ, Kim JS. Prediction of thermal expansion properties of carbon/epoxy laminates for temperature variation. *J Compos Mater* 2000;34(2):90–100.
- [33] Kim JH, Chang SH. Design of μ -CNC machining centre with carbon/epoxy composite-aluminium hybrid structures containing friction layers for high damping capacity. *Compos Struct* 2010;92(9):2128–36.
- [34] Zahlan N, Oneill JM. Design and fabrication of composite components - the spring-forward phenomenon. *Composites* 1989;20(1):77–81.